A Systematic Solution for the Problem of Spectral Degradation in Multiphase TX Architectures

Damir Hamidovic, *Student Member, IEEE*, Peter Preyler, *Student Member, IEEE*, Christoph Preissl, *Graduate Student Member, IEEE*, Mario Huemer, *Senior Member, IEEE*, and Andreas Springer, *Member, IEEE*

***Abstract*—With ever more stringent requirements of cellular standards it is an ongoing challenge to find the optimal RF transmitter architecture. In recent years, the multiphase transmitter (MP TX) architecture has been introduced as a promising candidate. It features high power efficiency and avoids phase modulation which is critical for upconversion of ultra-wideband signals. In this brief, the problem of unwanted spectral emission, inherent in MP TX architectures, is compensated by a proper data delay. Such an approach is considered for the first time in the multiphase architecture and achieves a spectral improvement of up to 38 dB in adjacent channels and 24 dB at the receiver (RX) duplex distance for a new radio (NR) signal with 20 MHz bandwidth. With the proposed solution the MP TX architecture becomes a highly competitive candidate for wideband signals such as LTE, LTE-CA or NR signals. In addition, a detailed and efficient implementation of the digital front-end (DFE) for the MP TX architecture including the proposed data delay is presented.**

***Index Terms*—Digital-intensive, transmitter, RF-DAC, DFE, multiphase, interpolation, delay.**

I. Introduction

AVOIDING analog signal processing in transmitters for wireless communications results in benefits such as decreased power consumption and good technology scaling. Therefore, polar [1]–[5] and IQ [6]–[9] digital-intensive wireless transmitter (TX) architectures, as well as novel hybrid approaches such as multiphase [10]–[13], outphasing [14], triphasing [15], or hybrid IQ-polar [16] are becoming a popular choice for today's and future wireless TX architectures. The major challenge of TX architectures is the up-conversion of the baseband (BB) signal to a specific radio-frequency (RF) band, in ideal case without any unwanted spectral components, with high power efficiency supporting wideband single carrier and carrier-aggregated signals.

Manuscript received March 22, 2021; revised May 12, 2021 and June 13, 2021; accepted July 3, 2021. Date of publication July 7, 2021; date of current version January 31, 2022. This work was supported in part by the Austrian Federal Ministry for Digital and Economic Affairs, in part by the National Foundation for Research, Technology and Development, and in part by the Christian Doppler Research Association. This brief was recommended by Associate Editor M. Yavari. *(Corresponding author: Damir Hamidovic.)*

The authors are with the Christian Doppler Laboratory for Digitally Assisted RF Transceivers for Future Mobile Communications, Johannes Kepler University Linz, 4040 Linz, Austria (e-mail: damir.hamidovic@jku.at; peter.preyler@jku.at; christoph.preissl@jku.at; mario.huemer@jku.at; andreas.springer@jku.at).

Color versions of one or more figures in this article are available at https://doi.org/10.1109/TCSII.2021.3095338.

Digital Object Identifier 10.1109/TCSII.2021.3095338

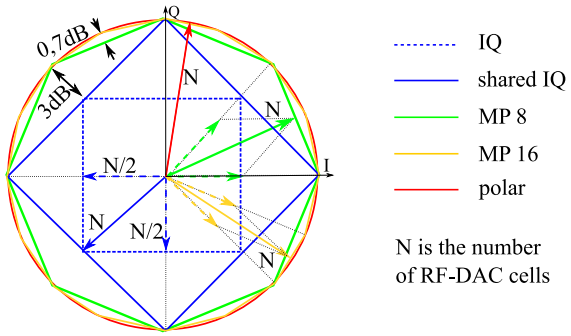

Fig. 1. Power efficiencies for different TX architectures.

The IQ architecture, on the one hand, has superior in-band (given as error-vector magnitude (EVM)), out-of band performance (given as unwanted spectral emission) and scalability for wide bandwidths, due to direct upconversion and linear combination of bandwidth-limited I and Q components. However, because of the summation of orthogonal components, the IQ architecture suffers from a maximal power efficiency drop of 3 dB, compared to polar, if a shared RF digital-to-analog converter (RF-DAC) is assumed [8]. Otherwise, the maximal power efficiency drop rises to 6 dB [17]. On the other hand, the polar architecture features a superior power efficiency but suffers from the nonlinear transformation from cartesian to polar coordinates, which is required, e.g., for long-term evolution (LTE) or new-radio (NR) standards, where in-phase and quadrature components of the BB data are generated [18]. Therefore, higher sampling rates are required because the phase and amplitude components occupy much wider bandwidths. Moreover, the digitally-controlled oscillator (DCO) tuning range and nonlinearity within the phase-locked loop (PLL) limit the signal bandwidth (BW) that can be upconverted [3].

For this reason, the focus of this brief is the multiphase (MP) TX architecture. Similar to the IQ architecture, it avoids a phase modulation of the carrier and overcomes the main disadvantage of the IQ architecture, which is the power efficiency drop. In terms of power efficiency, the MP architecture almost reaches the polar architecture. The main idea of the MP concept is to decrease the angle of the outphased components. This is possible if the two RF components can have two out of more than four phases of the local oscillator (LO) signal. Note that the IQ architecture has four possible LO phases. In order to establish a system where the RF components are outphased, e.g., by 45°, eight phases of the LO signal, outphased by 45° are needed, so that the RF components can

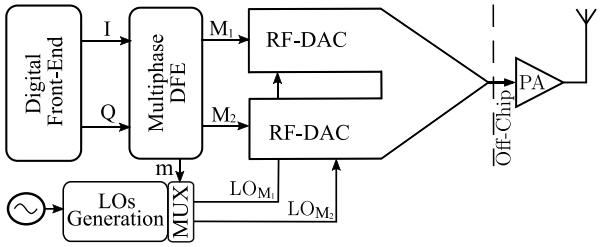

Fig. 2. A generic block diagram of the MP TX architecture, also used as a simulation setup. Blocks 'LOs Generation', 'RF-DAC' and 'Multiphase DFE' are presented in more detail in Figs: 3, 4 and 12, respectively.

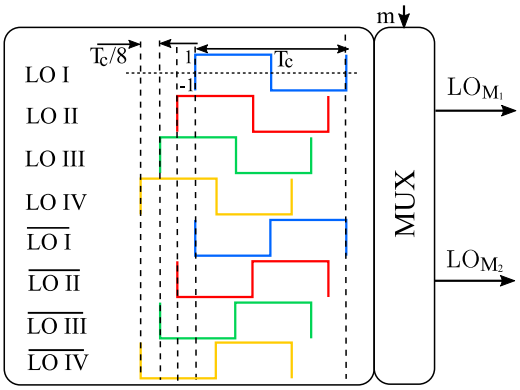

Fig. 3. 'LOs generation' block of the simulation setup where LO_{M_1} and LO_{M_2} are two adjacent LOs, chosen depending on the segment m, calculated in (2).

choose two adjacent LO phases to represent any sample on the constellation diagram. By increasing the number of possible phases the maximal power and efficiency drop of the RF-DAC is decreased from 3 dB to 0.7 dB for eight LO phases and to only 0.17 dB with 16 phases [10]. The visual presentation of the efficiency for IQ, polar and MP architectures, which can be obtained with the same number of RF-DAC power-cells N, is presented in Fig. 1. In this brief, an MP TX with 8 phases (MP8) is investigated, due to its good tradeoff between power efficiency and complexity.

A block diagram of the MP architecture is shown in Fig. 2. Several concepts for the LO generation for the MP architecture are presented in [19], [20]. However, a detailed implementation of the MP TX digital front-end (DFE) as one of the most important aspects of the new concept, has not been shown yet. Prior publications on the MP concept have optimized the architecture for high efficiency and thus the spectral performance is degraded due to a significant amount of out-of-band (OOB) noise [10]–[12]. Furthermore, the widest BW of the signal, upconverted with the MP TX architecture, showing spectral performance is only 10 MHz [10], [12]. Therefore, the focus of this brief is to investigate a systematic problem of unwanted OOB spectral emission, neglecting any implementation-related issue, and to propose a solution with significantly improved spectral performance. It will be shown for several different test-cases with signal BW up to 160MHz. Moreover, a detailed DFE implementation with the proposed concept will be presented.

II. Multiphase TX Working Principle

As mentioned, the main idea of the MP architecture is to gain in power efficiency and output power by having an

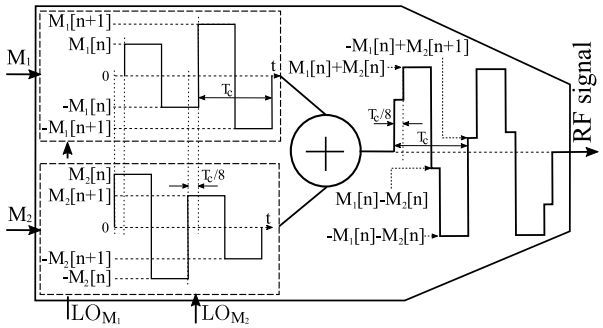

Fig. 4. Working principle of the block 'RF-DAC' from the simulation setup. LO_{M_1} and LO_{M_2} are scaled with magnitudes M_1 and M_1, respectively. The output RF signal is obtained as a sum of those two signals in time domain.

outphasing angle between the two RF components smaller than 90°. In order to achieve that, two LO signals with adjacent phases have to be chosen, depending on the angle of the complex BB data point in the constellation diagram. Those two LO signals are then mixed with two magnitude values M_1 and M_2 in the RF-DAC, which are calculated from the original IQ values as [10]

$$M_1 = \frac{I\sin\left(\frac{2\pi(m+1)}{M}\right) - Q\cos\left(\frac{2\pi(m+1)}{M}\right)}{\sin\left(\frac{2\pi}{M}\right)}, \tag{1}$$

$$M_2 = -\frac{I\sin\left(\frac{2\pi m}{M}\right) - Q\cos\left(\frac{2\pi m}{M}\right)}{\sin\left(\frac{2\pi}{M}\right)},$$

$$m = \left\lfloor \angle(I+jQ)\frac{M}{2\pi} \right\rfloor. \tag{2}$$

M represents the number of phases (in this work $M = 8$), and $0 \leq m < M$ is an integer value that determines the segment location of the current sample.

Multiphase TX With 8 Phases(A Simulation Setup): In this brief, the MP8 has been analyzed in a MATLAB-simulation setup, based on the block diagram from Fig. 2. In the block 'Digital Front-End' the BB data samples are generated. In 'Multiphase DFE' the generated BB data is upsampled to the carrier frequency f_c, and new magnitude values M_1 and M_2 and segment m are calculated based on (1) and (2) (details about the implementation of this block are presented in Section III). In the block 'LOs Generation' an LO-cycle for each of the 8 LOs is generated and two of those are chosen as the output LO_{M_1} and LO_{M_2} depending on the segment m, as shown in Fig. 3. Then every sample-pair $M_1[n], M_2[n]$ is mixed with an LO-cycle of a chosen pair of LOs LO_{M_1}, LO_{M_2}, respectively in the RF-DAC as presented in Fig. 4. LOs are simply scaled with the magnitude-values for each LO-cycle and summed up resulting in an output RF signal. The LO generation and mixing with data in the RF-DAC is simulated ideally, omitting the impact of phase noise [21], [22] and RF-DAC nonlinearity [23]. The focus is to emphasize the systematic problem of OOB spectral emission, discussed later in this section.

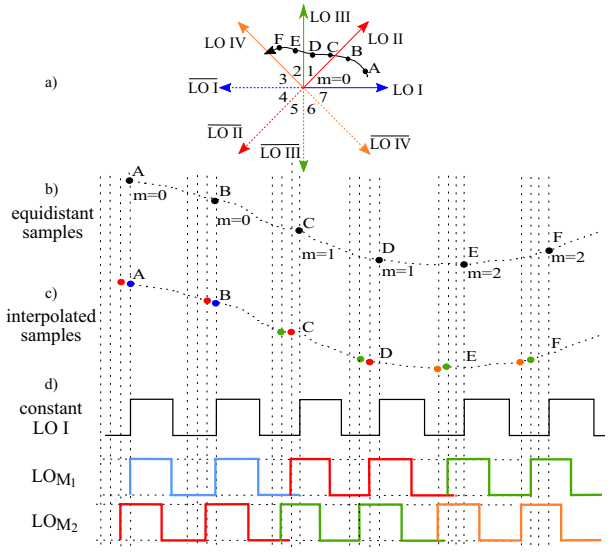

Fig. 5. Time domain signals in an MP8 TX for an example trajectory.

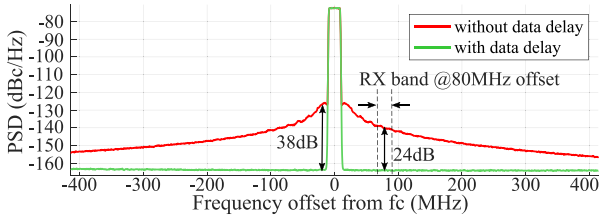

Fig. 6. PSD of an MP8 RF signal with and without data delay for an NR signal with 20 MHz BW at f_c=1.88 GHz in FDD band n2.

TABLE I
PSD COMPARISON FOR DIFFERENT TEST-CASES W/ AND W/O DATA DELAY ASSUMING IDEAL ANALOG CIRCUITRY

	OOB PSD [dBc/Hz]					
	Max.			at Δf		
	w/o D	w/ D	diff.	w/o D	w/ D	diff.
LTE 10 MHz at 1.8 GHz as in [10]	-129	-172	43	-149*	-172*	23
NR 20 MHz at 1.8 GHz as in Fig.6	-126	-164	38	-140*	-164*	24
QPSK BW 80 MHz at 5 GHz	-129	-162	33	-162$^+$	-141$^+$	21
QPSK BW 160 MHz at 5 GHz	-126	-153	27	-153$^+$	-131$^+$	22

D: data delay, *: Δf = 80 MHz, $^+$: Δf = 300 MHz.

A Systematic Problem Analysis

LOs with all possible phases are presented in Fig. 5a as vectors in the constellation diagram. Moreover, an example trajectory of the BB signal with 6 complex data points A, B, C, D, E and F in the constellation diagram is shown.

In Fig 5b, the magnitude of the example trajectory with equidistant-sampled data points (original IQ data) is presented. In Fig. 5d, LO$_{M_1}$ and LO$_{M_2}$ represent the resulting LO signals used for the multiphase components M_1 and M_2, respectively. It can be noticed that the edges of the LOs are shifted in time due to the phase difference between them. In most of RF-DAC-based architectures, the magnitude of an RF signal is updated with the rising and/or falling edges of the switching LO signal [24]. This means that magnitudes of the two MP components can be updated at different time instances, depending on the phases of currently used LOs. The simulated power spectral density (PSD) of the RF signal obtained by the upconversion of an NR signal with 20 MHz BW with an MP8 TX are shown in Fig. 6 in red color. The achieved OOB noise (-140dBc/Hz at RX frequency) is too high to fulfill the spectral requirements such as coexistence with other wireless standards and TX noise in RX band for FDD bands where, for a reference, state-of-the-art implementations achieve TX noise in RX band of <-157dBc/Hz [3].

In real circuit implementations, the OOB noise is dominated by RF-DAC nonlinearities in adjacent channels [23] and phase noise and/or quantization for far OOB spectrum [21]. This means that noise originated by any systematic limitation should be lower than noise originated by those effects. Although the mixing and LO generation are simulated ideally in this brief, a high noisefloor is observed, especially in adjacent channels. We have found that the root cause of this is the misalignment of the time instances at which the complex data points are sampled and the time instances where those data points are mixed with the LOs. As already mentioned, the original IQ data points are sampled on an equidistant grid (aligned with the rising edges of LO I), while the edges of different LOs (LO I - LO IV) are shifted in time for $\frac{T_c}{8}$, $\frac{T_c}{4}$ or $\frac{3T_c}{8}$, where $T_c = \frac{1}{f_c}$ and f_c is the carrier frequency. This results in mixing a magnitude, sampled at one time instance, with an LO at another time instance, thus updating the magnitude of the upconverted multiphase component at one time instance with a value from another time instance. This results in slightly wrong magnitudes of the output RF signal. A similar problem, with a detailed description of the root cause in the IQ system is presented in [24]. It is shown that in IQ systems, the problem arises because of the constant shift of the LO for I from the LO for Q by $\frac{T_c}{4}$, while both I and Q data are sampled on the same equidistant grid, aligned with the LO for I. In [24] it is shown that this systematic error results in an IQ image. Similarly, due to the same root cause, in MP TX a systematic error is present, which has not been identified and considered as a problem of OOB emission in prior MP implementations. The impact of the error in the MP TX is not only an IQ image, but also OOB emission. The reason for this is the dynamical switching between the LOs with different phases for both of the MP components, which can be seen as a coarse phase modulation, which is not present in the IQ system. Moreover, the magnitudes of the MP components, M_1 and M_2, have a broadband spectrum because of the nonlinear transformation (1). Therefore, any misalignment between M_1, M_2 and the LOs, including the one analyzed in this brief, results in broadband spectral emission. The solution in the IQ system is a simple delay of the Q data for the amount of $\frac{T_c}{4}$ [24]. Similarly, in the MP8 TX, M_1 and M_2 can be delayed by $\frac{T_c}{8}$, $\frac{T_c}{4}$ or $\frac{3T_c}{8}$, accordingly, in order to align the phase differences between the LOs and the magnitude data, mixed with the chosen LOs.

In this brief, the fractional delay is realized by a first order interpolation on the original IQ data, before the transformation from IQ to M_1 and M_2. The interpolation has been performed at the RF rate in order to avoid the upsampling of multiple interpolated streams of data. Since the first order interpolation is sufficient in order to significantly improve the spectral performance, it can be implemented very efficiently as it will be shown in the following section. Therefore, a higher order digital filter for delaying the data is not needed. The accordingly delayed data points are presented in Fig. 5c, where compared with Fig. 5d, it can be seen that the data points (on which the magnitudes M_1 and M_2 are calculated) are now

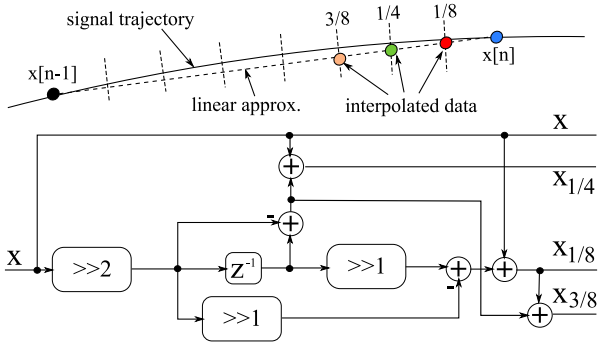

Fig. 7. An implementation of the data delay.

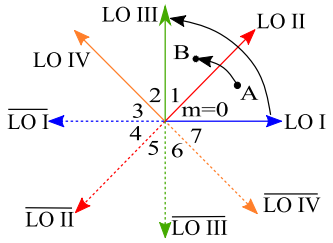

Fig. 8. The principle of separating LOs for M_1 and M_2. The LO for M_1 is LO I, LO III, $\overline{\text{LO I}}$ or $\overline{\text{LO III}}$. The LO for M_2 is LO II, LO IV, $\overline{\text{LO II}}$ or $\overline{\text{LO IV}}$.

TABLE II
PERFORMANCE COMPARISON FOR DIFFERENT TX ARCHITECTURES ASSUMING IDEAL ANALOG CIRCUITRY

NR signal with 20 MHz BW FDD band n2, f_c=1.88 GHz RX band @ Δf=80 MHz	polar concept from [25] w/o corr.	 w/ corr.	IQ [6] ideal*	**multiphase** **this work** w/o delay	 **w/ delay**
Max. efficiency drop+[dB]	0		3	0.7	
Max. OOB PSD [dBc/Hz]	-138	-184	$-\infty$*	-126	-164
PSD [dBc/Hz] @ RX band	-156	-184	$-\infty$*	-140	-164
LO-phase modulation	yes		no	coarse°	

+ efficiency drop due to outphasing of RF components, as shown in Fig. 1.
* the OOB noise of the IQ upconverted signal does not have systematic limitations. In real circuits it is limited by quantization [6], phase noise of LO generation circuitry [21] and RF-DAC nonlinearities [23].
° coarse modulation: switching between a few LOs with different phases.

aligned with the rising edges of the LOs used. The PSD of the RF signal obtained by the upconversion of the same BB signal, with applied data delay, is shown in Fig. 6 in green color where a significant improvement of the spectral performance compared to the MP8 TX without applied data delay is achieved. It can be seen that the improvement of the noisefloor is up to 38 dB in the adjacent channel and 24 dB in the RX band. Simulated PSD results for different test-cases, showing the improvement due to the data delay, are summarized in Table I. The OOB noise, after the data delay is applied, has a theoretical lower limit, caused by the third harmonic of the LO (carrier), which is typical for every phase-modulated signals, as explained in [14] for outphasing and [25] for polar architectures. In [25] is shown that this lower limit of the OOB noise is dependent on the ratio BW/f_c. An additional impact on the OOB noise in this brief is the usage of the first order interpolation instead of the ideal data delay. However, the theoretical lower limit has not been analyzed since a significant improvement has already been achieved. One test-case in Table I is the test case from [10]. Comparing the simulated results in Table I with the spectral results from [10], it can be concluded that in this specific test-case the dominant source of the OOB noise is not the misalignment analyzed in this brief, but SCPA nonlinearity and quantization noise due to optimization for efficiency, which degrades linearity. However, if the circuitry would be optimized for high linearity and different test-cases would be used, the impact of the discussed misalignment could limit the OOB PSD performance. In the MP architecture, the coarse phase modulation occurs due to switching between LOs with different phases. A performance comparison of different TX architectures is summarized in Table II.

III. MULTIPHASE DFE IMPLEMENTATION

Note that in the MP8, there are 4 different LOs (LO I-LO IV) and their inverted versions ($\overline{\text{LO I}} - \overline{\text{LO IV}}$), as shown in Fig. 3. Moreover, since time instances, where the original data is sampled, are aligned with one of the LOs (in this work LO I), only three additionally interpolated data streams, delayed by $\frac{T_c}{8}$, $\frac{T_c}{4}$ and $\frac{3T_c}{8}$, are needed. The delayed streams of data are calculated as

$$x_{1/8}[n] = \frac{7x[n] + x[n-1]}{8},$$
$$x_{1/4}[n] = \frac{3x[n] + x[n-1]}{4},$$
$$x_{3/8}[n] = \frac{5x[n] + 3x[n-1]}{8}. \quad (3)$$

An implementation of the data-delay is presented in Fig. 7. Only 3 bit-shifts, 5 adders and a register are needed in order to compute all 3 delayed data streams. In (1) the transformation from I, Q to M_1, M_2 is presented. For $M = 8$ these calculations can be significantly simplified.

Moreover, a principle of separating the LOs used for the component M_1 and LOs used for M_2 is introduced in this brief in order to reduce the number of LO switching when the signal trajectory changes to a neighboring segment. The principle is depicted in Fig. 8 where, in case of switching from point A to point B, LO_{M_1} switches from LO I to LO III, while the LO_{M_2} stays at LO II. With this principle, the LO used for LO_{M_1} is LO I, LO III, $\overline{\text{LO I}}$ or $\overline{\text{LO III}}$, and the LO used for LO_{M_2} is LO II, LO IV, $\overline{\text{LO II}}$ or $\overline{\text{LO IV}}$. Moreover, the calculations for M_1 and M_2 from (1) have to be mutually exchanged for every odd segment m, which yields the following simplifications

$$M_1 = ||I| - |Q||,$$
$$M_2 = \begin{Bmatrix} |Q| \cdot \sqrt{2}, & m = 0, 3, 4 \text{ or } 7 \\ |I| \cdot \sqrt{2}, & m = 1, 2, 5 \text{ or } 6 \end{Bmatrix}. \quad (4)$$

An implementation of the calculations of magnitude values M_1, M_2 from (4) and the segment number m from (2) are presented in Fig. 9. There is only one multiplication required for the implementation of M_2. However, it is a multiplication with a constant of value $\sqrt{2}$, where the constant can be coded with K bits, where $K < N - 1$, for a more efficient implementation without degrading the performance of the output signal. In Fig. 10 the entire MP DFE implementation is presented. It utilizes all the mentioned blocks in order to provide the properly aligned magnitude data for the two components M_1 and M_2 as well as the selection signal for the LOs for those two components. The selection signal in this brief is the segment number m.

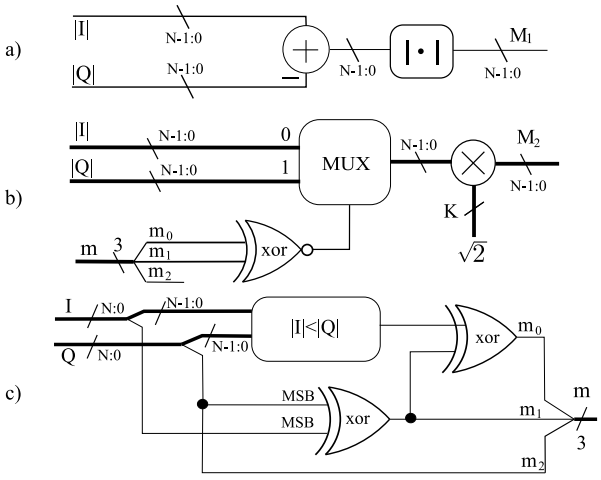

Fig. 9. An implementation for the calculation of a) M_1, b) M_2 and c) m.

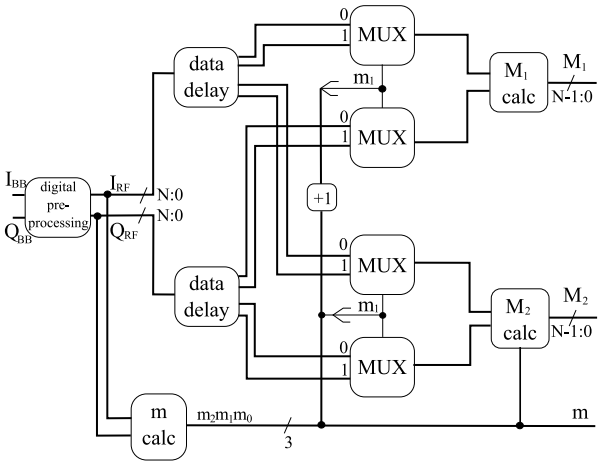

Fig. 10. An MP TX DFE implementation.

IV. Conclusion

In this brief, a concept for the removal of a systematic error, resulting in a significant improvement of the OOB spectrum up to 38 dB in the adjacent channel and 24 dB in the RX band at 80 MHz spacing by applying a proper data delay in the MP8 TX has been presented. This enables the usage of this architecture for wideband signals with high power efficiency and high output power, fulfilling the spectral requirements of today's and future wireless applications. Moreover, a detailed and efficient MP TX DFE implementation including the proposed data delay has been presented for the first time.

References

[1] Z. Boos *et al.*, "A fully digital multimode polar transmitter employing 17b RF DAC in 3G mode," in *Proc. IEEE Int. Solid-State Circuits Conf. (ISSCC)*, San Francisco, CA, USA, Feb. 2011, pp. 376–378.

[2] S.-M. Yoo *et al.*, "A switched-capacitor RF power amplifier," *IEEE J. Solid-State Circuits*, vol. 46, no. 12, pp. 2977–2987, Dec. 2011.

[3] M. Fulde *et al.*, "A digital multimode polar transmitter supporting 40MHz LTE carrier aggregation in 28nm CMOS," in *Proc. IEEE Int. Solid-State Circuit Conf. (ISSCC)*, San Francisco, CA, USA, Feb. 2017, pp. 218–219.

[4] P. Madoglio *et al.*, "A cellular multiband DTC-based digital polar transmitter with −153-dBc/Hz noise in 14-nm FinFET," *IEEE J. Solid-State Circuits*, vol. 55, no. 7, pp. 1830–1841, Jul. 2020.

[5] Y.-C. Choi, M. V. Lopez, S. Shin, S.-S. Yoo, and H.-J. Yoo, "A fully digital phase modulator with a highly linear phase calibration loop for wideband polar transmitters," *IEEE Trans. Circuits Syst. II, Exp. Briefs*, vol. 66, no. 2, pp. 222–226, Feb. 2019.

[6] M. S. Alavi, R. B. Staszewski, L. C. N. de Vreede, and J. R. Long, "A wideband 2x13-bit all-digital I/Q RF-DAC," *IEEE Trans. Microw. Theory Techn.*, vol. 62, no. 4, pp. 732–752, Apr. 2014.

[7] H. Wang *et al.*, "A highly-efficient multi-band multi-mode all-digital quadrature transmitter," *IEEE Trans. Circuits Syst. I, Reg. Papers*, vol. 61, no. 5, pp. 1321–1330, May 2014.

[8] H. Jin, D. Kim, and B. Kim, "Efficient digital quadrature transmitter based on IQ cell sharing," *IEEE J. Solid-State Circuits*, vol. 52, no. 5, pp. 1345–1357, May 2017.

[9] F. Zhang, P. Chen, J. S. Walling, A. Zhu, and R. B. Staszewski, "An active-under-coil RFDAC with analog linear interpolation in 28-nm CMOS," *IEEE Trans. Circuits Syst. I, Reg. Papers*, vol. 68, no. 5, pp. 1–14, May 2021.

[10] W. Yuan and J. S. Walling, "A multiphase switched capacitor power amplifier," *IEEE J. Solid-State Circuits*, vol. 52, no. 5, pp. 1320–1330, May 2017.

[11] Z. Bai, W. Yuan, A. Azam, and J. S. Walling, "Split-array, C-2C switched-capacitor power amplifiers," *IEEE J. Solid-State Circuits*, vol. 53, no. 6, pp. 1666–1677, Jun. 2018.

[12] Z. Bai, W. Yuan, A. Azam, and J. S. Walling, "A multiphase interpolating digital power amplifier for TX beamforming in 65nm CMOS," in *Proc. IEEE Int. Solid-State Circuits Conf. (ISSCC)*, San Francisco, CA, USA, Feb. 2019, pp. 78–79.

[13] M. Ma, F. You, Z. Xiao, T. Qian, Z. Tang, and S. He, "Design of multiphase class-G SCPA with enhanced efficiency," in *Proc. IEEE Int. Symp. Circuits Syst. (ISCAS)*, Oct. 2020, pp. 1–5.

[14] J. Lamberg *et al.*, "Digital interpolating phase modulator for wideband outphasing transmitters," *IEEE Trans. Circuits Syst. I, Reg. Papers*, vol. 63, no. 5, pp. 705–715, Mar. 2016.

[15] J. Lemberg *et al.*, "A 1.5–1.9-GHz all-digital tri-phasing transmitter with an integrated multilevel class-D power amplifier achieving 100-MHz RF bandwidth," *IEEE J. Solid-State Circuits*, vol. 54, no. 6, pp. 1517–1527, Jun. 2019.

[16] T. Buckel *et al.*, "A novel digital-intensive hybrid polar-I/Q RF transmitter architecture," *IEEE Trans. Circuits Syst. I, Reg. Papers*, vol. 65, no. 12, pp. 4390–4403, Dec. 2018.

[17] J. Zanen, E. Klumperink, and B. Nauta, "Analysis of switched capacitor losses in polar and quadrature switched capacitor PAs," *IEEE Trans. Circuits Syst. II, Exp. Briefs*, vol. 67, no. 10, pp. 1904–1908, Oct. 2020.

[18] A. Klinkan, E. Pfann, and M. Huemer, "A novel interpolation method for polar signals in radio frequency transmitters," *IEEE Trans. Circuits Syst. II, Exp. Briefs*, vol. 65, no. 5, pp. 692–696, May 2018.

[19] S. Sievert *et al.*, "A 2 GHz 244 fs-resolution 1.2 ps-peak-INL edge interpolator-based digital-to-time converter in 28 nm CMOS," *IEEE J. Solid-State Circuits*, vol. 51, no. 12, pp. 2992–3004, Dec. 2016.

[20] M. Kalcher and D. Gruber, "Self-aligned open-loop multiphase generator," in *Proc. IEEE Int. Symp. Circuits Syst. (ISCAS)*, May 2019, pp. 1–5.

[21] X. He and J. van Sinderen, "A low-power, low-EVM, SAW-less WCDMA transmitter using direct quadrature voltage modulation," *IEEE J. Solid-State Circuits*, vol. 44, no. 12, pp. 3448–3458, Dec. 2009.

[22] R. B. Staszewski and P. T. Balsara, "Phase-domain all-digital phase-locked loop," *IEEE Trans. Circuits Syst. II, Exp. Briefs*, vol. 52, no. 3, pp. 159–163, Mar. 2005.

[23] S. Trampitsch *et al.*, "A nonlinear switched state-space model for capacitive RF DACs," *IEEE Trans. Circuits Syst. I, Reg. Papers*, vol. 64, no. 6, pp. 1342–1353, Jun. 2017.

[24] J. Markovic, D. Hamidovic, C. Mayer, J. Zaleski, M. Huemer, and A. Springer, "An IQ image cancellation method for digital-intensive transmitters," in *Proc. IEEE Int. Symp. Circuits Syst. (ISCAS)*, May 2019, pp. 1–5.

[25] C. Preissl, P. Preyler, T. Mayer, A. Springer, and M. Huemer, "Analysis of spectral degradation and error compensation in 5G NR digital polar transmitters," *IEEE Trans. Circuits Syst. I, Reg. Papers*, vol. 67, no. 8, pp. 2719–2729, Aug. 2020.